ACS APPLIED MATERIALS & INTERFACES

Research Article

www.acsami.org

Graphene Oxide as a Water Dissociation Catalyst in the Bipolar Membrane Interfacial Layer

Michael B. McDonald and Michael S. Freund*

Department of Chemistry, University of Manitoba, Winnipeg, Manitoba R3T 2N2, Canada

Supporting Information

ABSTRACT: Bipolar membranes are formed by the lamination of an anion- and cation-exchange layer. Upon a sufficient applied reverse bias, water molecules at the layer junction dissociate, generating OH^- and H^+, which can be useful in electrodialysis and electrosynthesis applications. Graphene oxide has been introduced into bipolar membrane junctions (illustrated in the adjacent graphic) and is shown to be an efficient new water dissociation catalyst, lowering the overpotential by 75% compared to a control membrane. It was found that adjusting deposition conditions changes the nature of the graphene oxide films, leading to tunable membrane performance. Additionally, it is shown that their low overpotentials are stable, making for industrially viable, high-performance bipolar membranes.

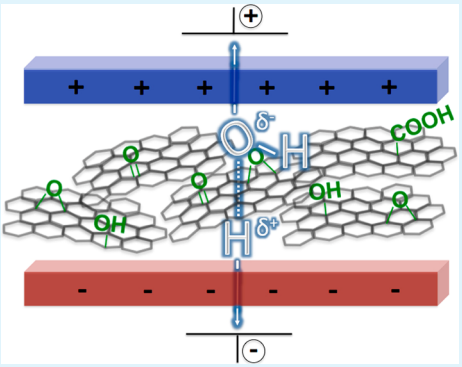

KEYWORDS: *graphene oxide, bipolar membrane, interfacial layer, water dissociation, catalysis*

INTRODUCTION

Bipolar membranes (BPMs) consist of an anion-exchange layer (AEL) laminated to a cation-exchange layer (CEL).[1] They have been shown to be analogous to *p*−*n* junction semiconductors, whereas the junction formed at the BPM interfacial layer (IL) constitutes a depletion region and thus contains a built-in potential.[2] When placed in an electrochemical cell under reverse bias conditions, like-charged electrolyte ions with respect to the membrane fixed charges (co-ions) are, to a large degree, blocked from traversing the membrane and can carry limited current depending on the layer permselectivity.[3] At potentials >0.83 V across the BPM, a very large electric field (10^8 V m^{-1}) is generated in the IL, and water molecules residing there become sufficiently polarized to dissociate.[4] The products of water dissociation (WD), OH^- and H^+, are therefore the major ionic current-carriers above 0.83 V, as OH^- migrates toward the anode and H^+ migrates toward the cathode.

As OH^- and H^+ concentrate in the respective compartments, a pH gradient is formed across the BPM−solution interfaces. This phenomenon appropriates a BPM to be incorporated in an electrosynthesis cell for the proton-coupled, electrochemical conversion of feedstock into value-added products, where the redox reactions are pH-dependent (Figure 1). Currently, in the most popular scenario, this has been exploited as an electrodialysis method to generate bases and acids from corresponding salt solutions (Figure SI-1a, Supporting Information).[5] Here, auxiliary ion-exchange membranes are incorporated to concentrate base and acid excreted from the BPM into the bulk solution.

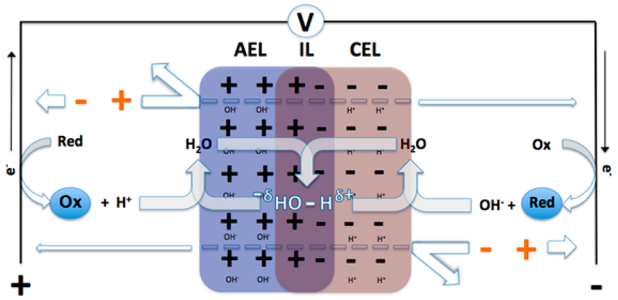

Figure 1. Scheme of a BPM under applied reverse bias sufficient to effect WD, depicting the general proton-coupled electrosynthesis of products (in blue circles) at both anode and cathode, and electron and ion transport. Charged products evolving from the redox reactions are balanced by the WD products. Feed solution counterions and co-ions (orange) migrate to the electrodes and the membrane (where most are electrostatically attenuated and some leak), respectively.

These membranes separate the feed solution, permeating only countercations to the AEL (base-generating) and counteranions to the CEL (acid-generating) compartments to balance OH^- and H^+. The feed and permeate solutions, and ion-exchange membranes, can also be switched to generate pure water from base and acid (Figure SI-1b, Supporting Information), although this has not yet been demonstrated. As a commercial endeavor, electrodialysis must perform efficiently

Received: May 23, 2014
Accepted: July 21, 2014
Published: July 21, 2014

Table 1. Characteristics of Ion-Exchange Membranes and BPMs

membrane	thickness (dry) (μm)	thickness (wet) (μm)	electrolyte resistance (Ω·cm^2)	WD product resistance (Ω·cm^2)
Nafion NR-211 (CEL)	20	20	0.4[a]	0.2[b]
Neosepta AHA (AEL)	180	190	19[c]	2.2[d]
AEL–CEL BPM	220	250	820[e]	65[f]
fumasep FBM	200	200	4600[e]	[23[f], 11[f]][g]

[a]Na^+. [b]H^+. [c]ClO_4^-. [d]OH^-. [e]Na^+ and ClO_4^- through entire membrane at current densities ~1 mA cm^{-2}. [f]H^+ and OH^- through entire membrane at current densities ~100 mA cm^{-2}. [g]Two different membranes; the latter equilibrated with 100 mA-cm^{-2} before collecting *J-E* data.

in terms of low co-ion crossover (competitive product purity) and energy consumption.[6]

Another use has been proposed involving BPMs as a means to maintain a pH gradient rather than build it, as OH^- and H^+ are consumed at the anode and cathode, respectively, and are recycled to the electrodes by WD in the absence of auxiliary membranes (Figure SI-1c, Supporting Information). This allows for processes such as water electrolysis across a BPM for hydrogen (fuel) production to occur simultaneously in two different pH conditions, which will provide more stable conditions for lower-cost, nonprecious metal electrodes and lower their overpotential.[7,8] The same application can be adapted using neutral electrolyte solution,[9] whereas charges generated at the gas-evolving electrodes are neutralized by the WD products (Figure SI-1d, Supporting Information). Like electrodialysis, for this process, the BPM should maintain the gradient indefinitely (low co-ion crossover) and pass current (WD) with minimized power input.

Catalysts have been included in the IL to impel WD, thereby reducing the overpotential to make BPM processes more energy efficient. Many examples of these studies are included in Table 1 of ref 7. Commercial BPMs are available and are produced on a large scale, exhibiting performance characteristics suitable for industrial application. The continuation and expansion of current BPMs will largely depend on their economic viability. Because ion-exchange layers have been intensively studied for many applications and are only responsible for BPM bulk charge transport,[10] better WD catalysts for the IL are sought to control the BPM potential to as close to the thermodynamic potential of 0.83 V as possible in order to lower energy consumption.

Graphene oxide (GO) is a nonspecifically oxidized derivative of graphene, which is composed of macromolecular, one atom-thick sheets of sp^2-hybridized carbon. Thus, a number of carbon sites are sp^3-hybridized with a variety of functional groups such as epoxide, carboxylate, and hydroxide.[11] As is the case with oxidatively activated graphite electrodes,[12] GO has been the subject of rigorous investigation recently for its use as an effective electrocatalyst for the oxygen reduction reaction (ORR) in fuel cells.[13] It has been shown that hydrogen bonding of bulk water in contact with oxide material surfaces induces proton transfer,[14] leading to a reduced activation barrier in the dissociation of water molecules.[15] Because of this general WD mechanism with oxides and because O–H bond reorganization in the presence of an electric field is also involved in the ORR, it is conceivable that GO may also be a WD catalyst. Inserting GO in the BPM IL offers a unique method of evaluating catalysts for this reaction in general.

In this work, BPMs have been prepared by the lamination of commercially available materials. The quality of these BPMs has been evaluated using microscopy, and their performance with and without GO in the IL were analyzed by the current density–voltage (*J–E*) relationship in 1 M electrolyte ($NaClO_4$) in water. The BPM properties were monitored for different GO deposition conditions, and the stability of these properties was assessed for successive experiments.

2. METHODS

2.1. Materials. Nafion NR-211 cation-exchange membrane was purchased from Ion Power, Inc. (New Castle, DE, USA); Nafion dispersion (10 wt %, aqueous) and graphene oxide (4 mg/mL, aqueous) were purchased from Sigma-Aldrich; Neosepta AHA anion-exchange membrane (Tokuyama America Inc.) was purchased from Ameridia (Somerset, NJ, USA); fumasep FBM was purchased from FuMA-Tech GmbH (St. Ingbert, Germany).

2.2. BPM Fabrication. BPMs were made by mounting 5 × 5 cm Neosepta AHA membranes flat to a glass substrate with tape. For GO–BPMs, GO solution (4, 2, or 1 mg/mL) was spin-coated (Headway Research, Garland, TX, USA) onto the membrane surface at various spin rates for 30 s, followed by heating in an oven at 110 °C for 2 min, to form AEL–GO. A Nafion contact layer was introduced by spin-coating two layers of Nafion aqueous dispersion on the AEL–GO surface at 500 rpm for 30 s, and heating in an oven at 110 °C for 2 min per layer. The bulk CEL was attached by adding 0.5 mL of Nafion dispersion to the spin-coated Nafion top layer and spreading a 6 × 6 cm Nafion NR-211 sheet (presoaked in water) across the membrane and overlapping the tape. Wrinkles and bubbles were squeegeed out by hand. The BPMs were dried in air overnight and then baked in a vacuum oven for 90 min at 110 °C. Lastly, the BPMs were cut at the tape boundaries to reveal well-adhered, flush edges.

2.3. Physical Characterization. Field emission scanning electron microscopy (FE-SEM) was performed on a JEOL JAMP-9500F field emission auger microprobe with 2.0 or 5.0 keV applied potential for qualitative observation as well as determination of IL thickness. Samples were cut using scissors and attached vertically with copper tape (3M) to view a cross-section. Dry and wet membrane thicknesses were measured using a Fowler Universal Electronic Micrometer.

2.4. *J–E* Measurements. Membrane potentials were evaluated by placing samples between two glass half-cells, each equipped with a primary solution container and separated Haber-Luggin capillary terminating at the flange, with a secondary container for reference electrodes. The cell-membrane contact was a custom thin (1 mm) gasket formed by casting solubilized electrical tape (BlueMagic) on the glass flanges. Electrochemical measurements were performed and recorded with a Solartron 1287 potentiostat in galvanostatic mode. Current densities between 0 and 120 mA cm^{-2} were applied in 20 min steps across the membrane in the primary solution compartments using Pt foil working electrodes (2 cm^2), and potential was measured using SCE electrodes in the Haber-Luggin capillary compartments. All *J–E* plots shown for BPMs in this work were performed under the conditions shown in Figure SI-1d (Supporting Information), with the AEL facing the anode and CEL facing the cathode, in 1 M $NaClO_4$.

3. RESULTS AND DISCUSSION

3.1. Characterization of Selected Ion-Exchange Membranes and Fabricated BPMs. The BPMs studied in this work were assembled using the commercially available Neosepta AHA anion-exchange membrane (AEL) and Nafion

NR-211 (CEL). The characteristics of the individual ion-exchange membranes used to form the anion- and cation-exchange layers of BPMs in this work, in addition to the resulting BPM characteristics, are summarized in Table 1. The AEL thickness is considerably larger than the CEL, which will form asymmetric BPMs, and so the AEL properties will dominate the mechanical and perhaps ion transport characteristics of the BPM. When hydrated, considerable swelling does not occur in either the AEL or CEL.

The individual ion-exchange layers have been laminated together to form a BPM, and the same measurements are shown in Table 1. The sum of the dry thicknesses of the AEL and CEL predicts a total thickness of 200 μm, and the measured dry thickness of the AEL−CEL BPM is 220 μm. The contact and adhesion layer therefore must account for ∼20 μm (10%) of the total BPM thickness. Unlike the individual membranes, when hydrated, the BPM swells significantly (>10%), implying physical rearrangement at the interface in this state. The fixed charges at the interface are no longer only electrically bound, as water interacts and relaxes the layer, opening the structure.[16]

To compare the ionic resistances of electrolyte counterions and WD products, two values have been measured for each individual ion-exchange membrane: that in neutral electrolyte (1 M $NaClO_4$) and that in extreme pH (1 M NaOH for AEL, 1 M $HClO_4$ for CEL), as these conditions will both be present in an electrodialysis process. The AEL will predominantly transport OH^- while the CEL will predominantly transport H^+. However, due to co-ion leakage, some amount of ClO_4^- will traverse the CEL and thus cross the AEL, and some Na^+ will traverse the AEL and thus cross the CEL. The AEL was found to have 1 order of magnitude greater resistance to anions than the CEL to cations, which is not surprising because Nafion is a leading material in cation conductivity.[17] The AEL used here was also 1 order of magnitude thicker than the CEL, which increases resistance. Both membranes are more resistive to electrolyte ions than OH^-/H^+, which can be explained on the basis of ionic radius and proton hopping.

AEL and CEL membranes (AEM and CEM, respectively) were laminated to form a BPM in the absence of an additional IL catalyst as a control. In this case, WD is catalyzed only by the ion-exchange groups near the layer interface.[18] When the BPM is placed with the AEL facing the anode and CEL facing the cathode (reverse bias) and a voltage is applied, the current is initially carried only by co-ions below a threshold bias, above which WD is effected. For this potential region, there is a resistance much larger (820 $\Omega\cdot cm^2$) than that of the electrolyte ions being transported through the individual ion-exchange layers (0.4, 19 $\Omega\cdot cm^2$). This difference is the resistance of co-ion leakage, which reflects the permselectivity (exclusion of co-ions) of the individual membrane layers. The resistance of Na^+ (ClO_4^-) against the positively (negatively) charged pores of the AEL (CEL) is substantial until reaching the CEL (AEL), which facilitates their transport.

At potentials where WD is initiated, the current is predominantly carried by the WD products through the AEL and CEL, respectively. The WD product resistance of AEL−CEL is an order of magnitude greater than the sum of the individual ion-exchange membranes. This difference can be attributed to the resistance of WD to generate and transport OH^-/H^+ in this particular IL, which is expected to require more potential than simply moving charges through a resistor.

As a comparison to commercially available, industrially manufactured BPMs, the same measurements were conducted on the BPM fumasep FBM (Table 1). Its thickness is similar to that of AEL-CEL, but does not swell when hydrated. This attests to the higher quality of fabrication than can be achieved for BPMs made in this study, as this feature indicates that there is no reorganization of the structure or delamination of the IL upon hydration, unlike AEL−CEL. Its co-ion resistance is 1 order of magnitude greater than AEL−CEL, demonstrating superior permselectivity properties of the system (both ion-exchange layers and junction structure). The OH^-/H^+/WD resistance is significantly decreased versus AEL−CEL, which can be due to superior ion-exchange materials selected for OH^-/H^+ transport and/or an IL more capable to perform WD and transfer its products.

The morphology of the BPMs used in this work is shown in Figure 2. The cross-section FE-SEM images exhibit the distinct layered structure of these membranes, including the features of the AEL, CEL, and IL. Figure 2a reveals four distinguishable layers for fumasep FBM, at least one layer more than is expected to be observable. Because details of the materials or methods of manufacture of the commercially available BPM are not known, assignment of the layers in terms of the BPM are unclear. The overall structure is very heterogeneous, with minimal interlayer entanglement, making for a uniform thickness of each layer. This has been shown to be ideal for WD and charge transport in BPMs.[19,16]

The AEL−CEL membrane is shown in Figure 2b. Unlike fumasep FBM, the AEL contains a cracked, heterogeneous structure of Neosepta AHA pieces with grain boundaries. From left to right (toward the middle of the cross-section), the AEL becomes more singular, eventually culminating at the AEL−CEL junction with the smoother spin-coated Nafion layers. At the right-most side of the image is the laminated Nafion sheet, forming the bulk of the CEL. This preformed Nafion appears very different than the wet-deposited Nafion adhesion layers. Figure 1b highlights the asymmetry of the BPMs used in this study, as the AEL−CEL junction is much closer to the CEL side.

Overall, the structure formed is significantly less neat than fumasep FBM, with a less intimate contact formed within the layers (Figure 2b inset), which hypothetically makes for a less ideal structure for WD and charge transport.

3.2. Effect of GO IL. An advantage of GO is that it is water-soluble, making it appropriate for this process, as it will form homogeneous, uniform layers, which is important for a BPM IL.[19] GO was added to the BPMs using the same methods as those to construct the structure in Figure 1b, to form GO−BPMs, shown in Figure 2c. The contact formed with the CEL appears to be very good, with a flush interface as a result of the Nafion adhesion layer harmonizing with GO better than the Neosepta AHA membrane (Figure 2b inset). However, like AEL−CEL, GO does not make a neat interface with Neosepta AHA. This is likely due to the hydrophobicity of this membrane in the dry state, and so the aqueous Nafion and GO do not make intimate contact under the spin-coating conditions employed in this work. The overall structure is improved relative to AEL−CEL, but the layer contact is not apparently as advanced as the commercial BPM. Because the WD and immediate OH^-/H^+ transport events occur at the IL, the structural uniformity between the AEL−GO and GO−CEL junctions will dominate the electrical properties of the BPM.

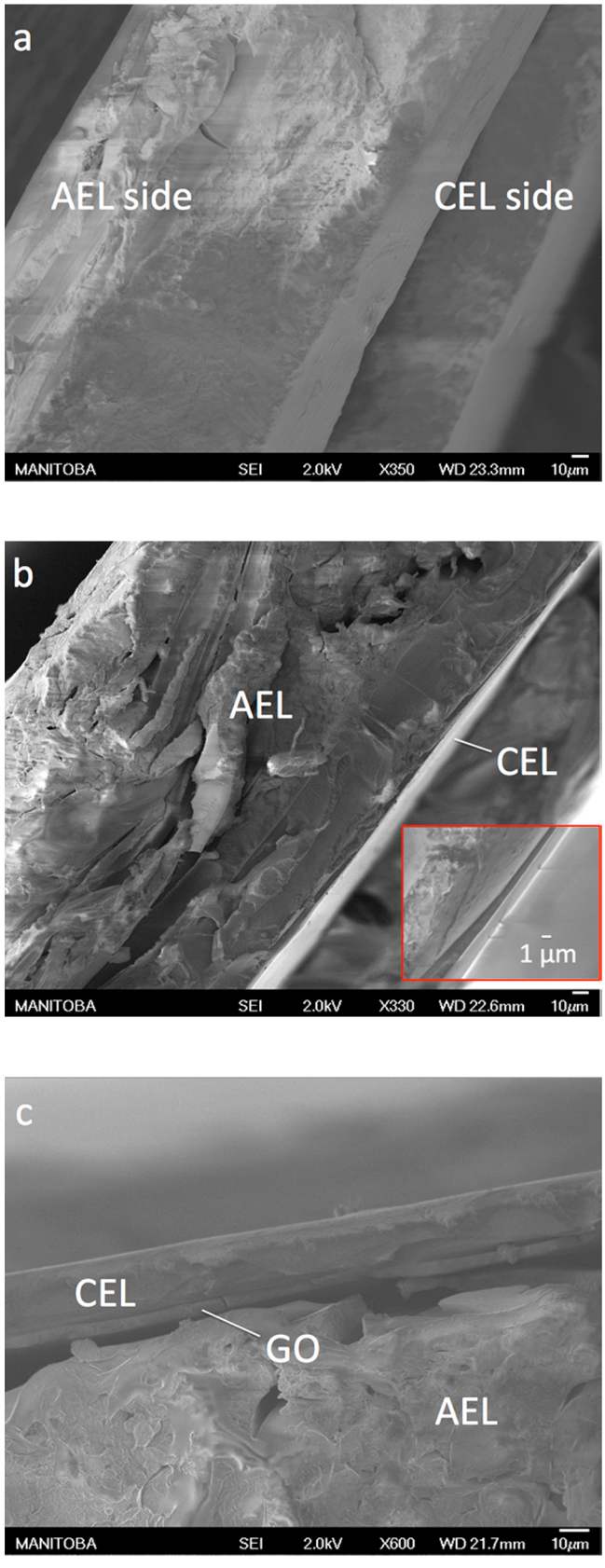

Figure 2. Cross-sectional FE-SEM images of (a) fumasep FBM, (b) AEL-CEL (inset: layer junction), and (c) GO–BPM (4 mg/mL, 500 rpm).

The current density–potential (J–E) relationship reveals the critical elements of BPMs such as the overall permselectivity, water dissociation overpotential, and membrane resistance.[6] The general BPM J–E curve has been examined in detail previously[20] and is composed of regions characterized by current carried by co-ions due to leakage and OH^-/H^+ transport due to WD.

With the same neutral electrolyte solution at both the anode/AEL and cathode/CEL (Figure SI-1d, Supporting Information), some currents (<1 mA cm^{-2}) are carried by co-ions because the ion-exchange layer permselectivities are nonideal. The maximum rate of co-ion leakage is indicated by a very resistive region of the curve known as the "first limiting region"[1] where the current is independent of potential. Thus, it is an indicator of the overall permselectivity of the BPM, as the maximum current density of this region can be used to calculate the co-ion leakage rate (see section SI-4, Supporting Information). With a greater leakage-limited current density, larger amounts of co-ions are able to leak across the BPM, and it is therefore less permselective. This region exists until the applied bias induces a sufficient electric field such that WD is activated (E_{WD}) and OH^- and H^+ carry charge ohmically for reasonably high current densities (>100 mA cm^{-2}). The difference between the thermodynamic potential (0.83 V) and experimentally measured potential will quantify the catalytic effectiveness of the IL. This overpotential can be registered at applied biases associated with typical electrodialysis processes, such as that at 100 mA cm^{-2} (E(100)).

The J–E relationship of BPMs examined in this work and the figures of merit described have been extracted in Figure 3 and

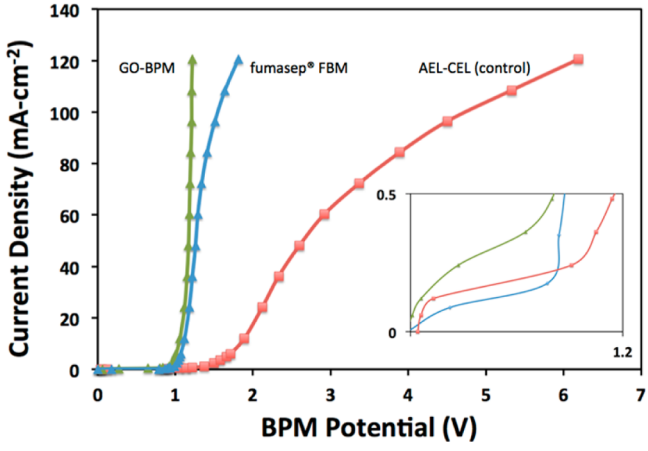

Figure 3. J–E relationship of a current-conditioned fumasep FBM (blue), AEL–CEL control BPM (red), and GO–BPM made by spin-coating 2 mg/mL GO solution at 500 rpm.

Table 2, respectively. The commercial BPM fumasep FBM sets precedent for the response of an optimally manufactured BPM performing electrodialysis in 1 M $NaClO_4$. As seen in Figure 3 inset, the limiting region resides at very low currents (<0.1 mA cm^{-2}), indicating good permselectivity and hence higher maximum acid and base product purity. With co-ion crossover <1 nmol s^{-1} cm^{-2}, this translates to a purity of 99.945%, which is better than that of the average BPM capability (99%)[6] and sets a standard for permselectivity of these BPMs. The on-set of current, corresponding to the initiation of WD, occurs at 0.8 V. This is close to the thermodynamic value of 0.83 V, denoting that commercial membranes effectively catalyze WD with

Table 2. Figures of Merit for Commercial and Lab-Made BPMs from Figure 3

membrane	permselectivity ($nmol_{co\text{-}ion}$ s^{-1} cm^{-2})	maximum product purity (%)	E_{WD} (V)	R_{WD} ($\Omega \cdot cm^2$)	E(100) (V)
fumasep FBM	0.6	99.945	0.8	23, 11[a]	2.4, 1.6[a]
AEL−CEL BPM	1.3	99.875	0.9	65	4.7
GO−BPM	2.3	99.774	0.8	0.6	1.2

[a]Two different membranes; the latter was equilibrated with 100 mA cm^{-2} before collecting J−E data yielded permselectivity and E_{WD}, which was not significantly different, but R_{WD} and thus E(100), which was very different.

minimal overpotential at low current densities. The resistance of the system when WD is being effected, R_{WD}, is considerable for one membrane (not shown in Figure 3), leading to a required voltage for electrodialysis (E(100)) of 4.7 V. The measured values for fumasep FBM depend on the treatment of the membrane prior to making the measurement. For example, the second values listed in Tables 1 and 2 were made after applying a current density of 100 mA-cm^{-2} for 3 h ("current-conditioning"), then turning off the current and allowing the open circuit voltage to reach equilibrium before beginning J-E measurements. This treatment results in significantly less overpotential for fumasep FBM (1.6 V). As seen in Figure 3, the slope of this curve decreases visibly as current densities increase toward 100 mA cm^{-2}, indicating that higher current densities would require significantly more overpotential.

BPMs fabricated without the sophisticated resources of industrial manufacturing likely have inferior characteristics due to inferior ILs (WD catalysts) and/or unoptimized fabrication methods being employed. This is evident in the control BPM AEL−CEL. In the absence of an added WD catalyst, the BPM characteristics are presumably due to only the ion-exchange layers and the nature of the interface of the ion-exchange layers selected for this study. The leakage of co-ions is twice that of fumasep FBM, leading to a decreased maximum product purity of 99.875%. Additionally, it is more resistive, with an overpotential of 4.7 V at 100 mA cm^{-2}. Thus, as expected, the quality of its figures of merit are poor compared to those of commercial BPMs.

With the incorporation of GO in the IL, the measured permselectivity and product purity of GO−BPM are significantly poorer than those of AEL−CEL, indicating that, as observed in a previous report, even the relatively thin IL plays a considerable role in membrane transport properties.[21] Although this is detrimental, it is conceivable that this may be overcome by optimizing the GO deposition and layer assembly methods. In contrast, the observed overpotential is only 1.2 V, compared to 1.7 V for fumasep FBM under the best conditions, and a decrease of 75% versus AEL−CEL. E_{WD} is decreased from 0.9 V for AEL−CEL to near the thermodynamic value (0.8 V). Remarkably, R_{WD} is nearly insignificant. Unlike fumasep FBM, which commences becoming more resistive at current densities ~100 mA cm^{-2}, the GO−BPM remains ohmic and thus is not limited by water transport to the interface at high current densities.[22] This demonstrates that GO is an efficient WD catalyst and that the a GO IL enhances the transport of water, OH^-, and H^+ exceptionally.

3.3. Effect of GO Deposition Conditions. Studies on GO morphology focus principally on primary structure,[23] while there is a lack of in-depth knowledge regarding the arrangement of individual molecules into bulk films[24] using wet techniques such as spin-coating adopted in this work. The shortcomings in understanding spin-coated GO films presents the opportunity to conveniently alter the bulk GO structure for the purpose of tuning catalytic performance. Modifying conditions such as the spin-coat rate and GO solution concentration can potentially translate into the modulated arrangement of individual GO sheets, extending to changes in GO−BPM electrical behavior. This study was performed and the impact on the J−E characteristics is shown Figure 4, with figures of merit summarized in Table 3.

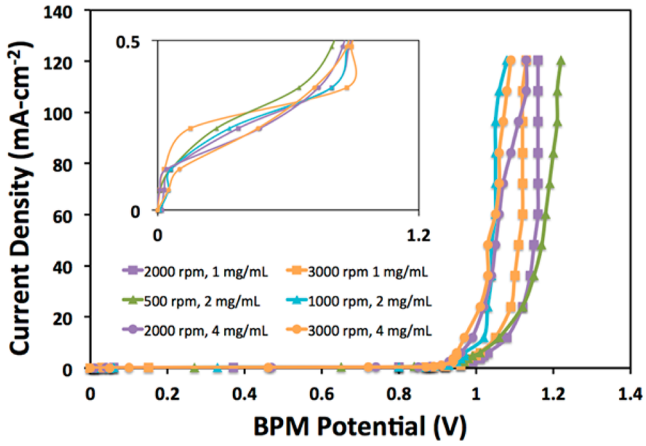

Figure 4. J−E relationship of GO−BPMs fabricated under different GO-deposition conditions (spin-coat rate and GO solution concentration). Inset: focus on limiting current density regions.

In general, it is assumed that the deposited films will be thinner with increased spin-coat rates and lower GO solution concentration. The resulting film thicknesses (Table 3) as a function of these two parameters do not consistently develop intuitively. Although, overall, the GO films are generally thinner at higher spin-coat rates, for constant solution concentrations, in the case of 2 and 4 mg/mL GO solutions, the thickness increases at higher spin-coat rates. The spin-coat rate dominates the final film thickness achieved, as it is independent of GO solution concentration (Figure SI-3, Supporting Information).

Because the only distinction is the structure of the GO IL, this is reasonably the only contributing factor to differences in J−E behavior of the GO−BPMs investigated. Overall, the permselectivity of the GO−BPM does not change considerably as a function of film thickness (Figure SI-4a, Supporting Information). This is because the much thicker ion-exchange layers dominate ion transport rather than slight changes to the structure of the relatively thin IL. There is also no correlation to permselectivity and the films formed under different spin-coat rates or GO solution concentration, independent of each other (Figure SI-4b, Supporting Information).

The R_{WD} value shows no discernible correlation as a function of thickness achieved or spin-coating rate (Figure SI-5a,b, Supporting Information). There is also not a consistent effect on this feature as a function of GO solution concentration; however, it is noteworthy that the lowest concentration of GO starting material (1 mg/mL) produced the lowest R_{WD} values,

Table 3. Figures of Merit for GO-BPMs from Figure 4

GO concentration (mg/mL)	spin-coat rate (rpm)	thickness (μm)	permselectivity ($nmol_{co\text{-}ion}$ s^{-1} cm^{-2})	R_{WD} ($\Omega \cdot cm^2$)	E(100) (V)
1	2000	0.14 ± 0.05	2.0	0.0	1.16
1	3000	0.07 ± 0.01	1.9	0.4	1.12
2	500	0.7 ± 0.2	2.3	0.6	1.21
2	1000	1.0 ± 0.4	2.0	1.0	1.05
4	2000	0.09 ± 0.03	2.2	1.3	1.12
4	3000	0.21 ± 0.03	2.2	0.8	1.07

independent of spin-coat rate, and this trend is true for all except one GO−BPM (4 mg/mL, 3000 rpm). This implies a difference in film structure for lower concentrations of GO, leading to improved transport behavior, regardless of thickness.

The overall overpotential at 100 mA cm^{-2} E(100) shows anomalous behavior as a function of thickness that can also be ascribed to properties granted upon film formation under different conditions (Figure SI-6, Supporting Information). The lowest overpotentials were observed for films made at the higher concentrations of 2 and 4 mg/mL, specifically for higher spin-coat rates, and thus the film structure formed dominates over thickness. This indicates that films formed from higher GO concentrations and faster spin-coating generate ILs that facilitate overall WD and product transport the most effectively, which is, unexpectedly, the opposite to the observations of R_{WD}. Due to the overall lack of correlation between the parameters and measured figures of merit, the control afforded by spin-coat rate and GO solution concentration is not reliable. However, these parameters do apparently render diverse film structures that possess qualities suitable to optimizing the GO IL for WD.

3.4. Stability of GO−BPMs. It is important that BPM qualities remain stable as a function of operating time, which will determine their longevity in operation. This will factor into cost and thus feasibility for industrial translation of the technology. Figure 5 shows the change in BPM permselectivity and E(100) as a function of the number of times a single membrane was subjected to the applied currents involved in the *J*−*E* experiments undertaken in this work. This includes applied current densities of and greater than 100 mA cm^{-2} for 2 h, which is relevant to industrial magnitudes.

As the permselectivity determines the attainable product purity in processes such as acid and base production, this quality would ideally remain consistent throughout the lifetime of a BPM. Figure 5a shows the co-ion leakage value as a function of number of experimental runs for the AEL−CEL control BPM, which, in the absence of a heterogeneous IL, reflects primarily the change in permselectivity of the ion-exchange layers. Although fluctuation is significant, over four runs the membrane leakiness did not change overall and not detrimentally so. This is expected for the electrostatic aspects of the pore phase of polymer membranes that repel co-ions, as well as the structural phase, which should remain robust and impermeable to solution crossover.[10]

When a GO IL is introduced (Figure 5b), the overall leakage increases by 1 order of magnitude over the course of six runs, and levels off after five runs. Therefore, although leakage becomes greater for the GO−BPM, the permselectivity stabilizes over reasonable amounts of time. This behavior can be explained by rearrangement of the GO structure under a very large electric field,[25] where the dipoles on oxygenic groups on GO are very strongly influenced by the direction of the field,[26] the neighboring fixed charges on the ion-exchange layers, and the dipoles of neighboring GO sheets. After

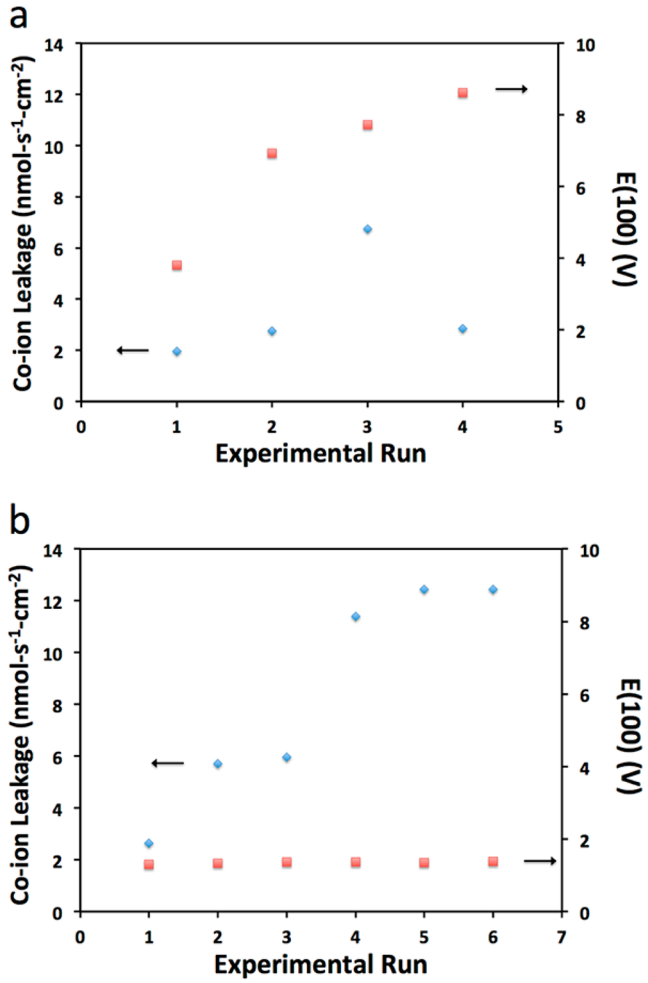

Figure 5. Permselectivity and E(100) for successive *J*−*E* experiments carried out on the same membrane, for (a) CEL−AEL and (b) GO−BPM (2 mg/mL, 500 rpm).

sufficient time under these conditions, the sheets presumably align in the most favorable arrangement. In this case, the final arrangement allows for more leakage of co-ions across the BPM junction, likely because rapid generation of OH^- and H^+ force a more open structure for their immediate transport to the ion-exchange layers. Thus, the GO IL plays a significant role in co-ion leakage over operating time.

It is important that the voltage required for processing conditions also be stable in order to provide consistent power consumption. It was shown in section 3.2 that the primary benefit of the GO catalyst is to lower the input energy required, reducing cost, and GO-BPMs should be capable of this in the long term. In the absence of GO, E(100) for AEL−CEL is shown in Figure 5a, which expresses predominantly the resistance of the ion-exchange layers to OH^-/H^+ (as opposed

to only co-ions) and that of water dissociation at their junction. This value increases to more than twice its original value over four runs, from <4 to >8 V, which translates to a doubling in energy consumption. Because the permselectivity experiment did not show evidence of change to co-ion transport, it is unlikely that the ion-exchange layers are affected so as to influence the transport of OH^-/H^+. This indicates that the drastic decrease in performance is related to changes in the junction structure. Because there are no added materials to the IL, it is possible that the large electric field and rapid reaction in this region causes physical defects such as delamination, which disrupts a continuous space charge layer, raising the voltage required to dissociate water. Chemical defects are also possible, as the water dissociation is catalyzed by the interfacial ion-exchange groups bound to the membrane layers in this BPM,[18] causing a decrease in the electric field produced in the IL at a given applied potential.

E(100), as a function of experimental exposure, is shown in Figure 5b in the presence of a GO IL. Unlike the control BPM, the GO−BPM potential does not change appreciably over six runs, indicating that the efficiency granted for this BPM is stable. Because it is already shown in Figure 5a that the BPMs prepared in this study are affected at their junction and not their ion-exchange layers, and the GO−BPM overpotential is stable whereas the control BPM is not, it is the presence of GO that enhances stability of the IL. In congruence with the rationale given for the diminishing performance of the control BPM, it is possible that the GO layer provides improved adhesion to the ion-exchange layers, keeping the trilayer, and thus the space charge region, intact for superior water and product transport. Chemical damage caused by WD reactions occurring in conjunction with ion-exchange layer groups at the interface is also mitigated, because GO is the dominant catalyst.

4. CONCLUSION

BPMs have been prepared in the presence and absence of a GO IL and their performance characterized in terms of their permselectivity and overpotential. GO was found to be an excellent WD catalyst that minimizes BPM resistance to all aspects of this process and stabilizes the enhanced operation over time, with inexpensive and facile film-forming properties. It was found that the GO deposition conditions investigated herein do not control the thickness intuitively, but can alter the film structure to potentially optimize WD figures of merit. GO−BPMs with films formed using higher concentrations of GO and faster spin-coat rates grant lower overpotentials at current densities relevant to industrial applications.

Because the adhesion and general interaction between GO and the ion-exchange layers will be a determining factor in the IL quality and stability, and noting that the experiments conducted herein are based on nonoptimally manufactured BPMs, it is likely that if the fabrication process is developed and industrialized, both the permselectivity and overpotential will improve more so, and become more stabilized for long-term operation. Investigation of the chemical and morphological structure, other film-forming conditions, and a broader range of thicknesses will potentially advance the control and achievable potency of the GO IL. The use of spin-coat deposition provides an easily variable and inexpensive tool for achieving this as well as other practicality aspects. Use of other ion-exchange materials may also improve the GO−BPM.

The ramifications of the GO−BPM will lead to larger operating current densities due to the lower overpotential, leading to faster, less expensive, and more efficient electrodialysis and water electrolysis processes. In a broader context, fundamental understanding into the workings of GO as a WD catalyst should be studied further as it may have a role in enriching other relevant reactions, processes, and important applications.

■ ASSOCIATED CONTENT

Supporting Information

Schemes of BPMs in applications; images of ion-exchange membranes; membrane resistance calculation; permselectivity calculation; product purity calculation; E_{WD}, R_{WD}, and E(100) calculation, correlation of permselectivity, R_{WD}, and E(100) to GO deposition conditions. This material is available free of charge via the Internet at http://pubs.acs.org.

■ AUTHOR INFORMATION

Corresponding Author

*M. S. Freund. E-mail: michael_freund@umanitoba.ca.

Notes

The authors declare no competing financial interest.

■ ACKNOWLEDGMENTS

The authors acknowledge support by the Natural Sciences and Engineering Research Council (NSERC) of Canada, the Canada Research Chair program, the Province of Manitoba's Science and Technology International Collaboration Fund, and the University of Manitoba. This research made use of the Manitoba Institute for Materials (MIM) facility, which is supported by the Canada Foundation for Innovation (CFI), the Manitoba Research and Innovation Fund, and the University of Manitoba. The authors thank MIM Electron Spectroscopy and Microscopy Facility supervisor Abdul Khan (MIM) for help in FE-SEM imaging.

■ REFERENCES

(1) Strathmann, H. Electrodialysis, A Mature Technology with a Multitude of New Applications. *Desalination* **2010**, *264*, 268−288.
(2) Ramírez, P.; Rapp, H. J.; Reichle, S.; Strathmann, H.; Mafé, S. Current-Voltage Curves of Bipolar Membranes. *J. Appl. Phys.* **1992**, *72*, 259−264.
(3) Balster, J.; Sumbharaju, R.; Srikantharajah, S.; Pünt, I.; Stamatialis, D. F.; Jordan, V.; Wessling, M. Asymmetric Bipolar Membrane: A Tool to Improve Product Purity. *J. Membr. Sci.* **2007**, *287*, 246−256.
(4) Mafé, S.; Ramírez, P.; Alcaraz, A. Electric Field-Assisted Proton Transfer and Water Dissociation at the Junction of a Fixed-Charge Bipolar Membrane. *Chem. Phys. Lett.* **1998**, *294*, 406−412.
(5) Tongwen, X. Electrodialysis Processes with Bipolar Membranes (EDBM) in Environmental Protection—A Review. *Resour., Conserv. Recycl.* **2002**, *37*, 1−22.
(6) Wilhelm, F. G.; Pünt, I.; van der Vegt, N. F. A.; Wessling, M.; Strathmann, H. Optimisation Strategies for the Preparation of Bipolar Membranes with Reduced Salt Ion Leakage in Acid−Base Electrodialysis. *J. Membr. Sci.* **2001**, *182*, 13−28.
(7) McDonald, M. B.; Ardo, S.; Lewis, N. S.; Freund, M. S. Use of Bipolar Membranes for Maintaining Steady-State pH Gradients in Membrane-Supported Solar-Driven Water-Splitting. *ChemSusChem* **2014**, submitted.
(8) Vargas-Barbosa, N. M.; Geise, G. M.; Hickner, M. A.; Mallouk, T. E. Assessing the Utility of Bipolar Membranes for Photoelectrochemical Water-Splitting Cells. *ChemSusChem* **2014**, submitted.
(9) Hung, C.-Y.; Li, S.-D.; Wang, C.-C.; Chen, C.-Y. Influences of a Bipolar Membrane and an Ultrasonic Field on Alkaline Water Electrolysis. *J. Membr. Sci.* **2012**, *389*, 197−204.

(10) Xu, T. Ion Exchange Membranes: State of their Development and Perspective. *J. Membr. Sci.* **2005**, *263*, 1−29.
(11) Mao, S.; Pu, H.; Chen, J. Graphene Oxide and Its Reduction: Modeling and Experimental Progress. *RSC Adv.* **2012**, *2*, 2643−2662.
(12) McCreery, R. L. In *Electroanalytical Chemistry*; Bard, A J., Ed.; Elsevier: Dekker, NY, 1991; Vol. *17*, pp 221−374.
(13) Huang, C.; Li, C.; Shi, G. Graphene Based Catalysts. *Energy Environ. Sci.* **2012**, *5*, 8848−8868.
(14) Tocci, G.; Michaelides, A. Solvent-Induced Proton Hopping at a Water−Oxide Interface. *J. Phys. Chem. Lett.* **2014**, *5*, 474−480.
(15) Hass, K. C.; Schneider, W. F.; Curioni, A.; Andreoni, W. The Chemistry of Water on Alumina Surfaces: Reaction Dynamics from First Principles. *Science* **1998**, *282*, 265−268.
(16) Simons, R. Preparation of a High Performance Bipolar Membrane. *J. Membr. Sci.* **1993**, *78*, 13−23.
(17) Slade, S.; Campbell, S. A.; Ralph, T. R.; Walsh, F. C. Ionic Conductivity of an Extruded Nafion 1100 EW Series of Membranes. *J. Electrochem. Soc.* **2002**, *149*, A1556−A1564.
(18) Simons, R. Water Splitting in Ion Exchange Membranes. *Electrochim. Acta* **1985**, *30*, 275−282.
(19) Strathmann, H.; Krol, J. J.; Rapp, H. J.; Eigenberger, G. Limiting Current Density and Water Dissociation in Bipolar Membranes. *J. Membr. Sci.* **1997**, *125*, 123−142.
(20) Ramírez, P. R. H. J.; Mafé, S.; Bauer, B. Bipolar Membranes under Forward and Reverse Bias Conditions. Theory vs. Experiment. *J. Electroanal. Chem.* **1994**, *375*, 101−108.
(21) Abdu, S.; Sricharoen, K.; Wong, J. E.; Muljadi, E. S.; Melin, T.; Wessling, M. Catalytic Polyelectrolyte Multilayers at the Bipolar Membrane Interface. *ACS Appl. Mater. Interfaces* **2013**, *5*, 10445−10455.
(22) Krol, J. J.; Jansink, M.; Wessling, M.; Strathmann, H. Behaviour of Bipolar Membranes at High Current Density: Water Diffusion Limitation. *Sep. Purif. Technol.* **1998**, *14*, 41−52.
(23) Zhang, S.; Zhou, J.; Wang, Q.; Jena, P. Structure, Stability, and Property Modulations of Stoichiometric Graphene Oxide. *J. Phys. Chem. C* **2013**, *117*, 1064−1070.
(24) Wood, C. D.; Palmeri, M. J.; Putz, K. W.; An, Z.; Nguyen, S. T.; Catherine Brinson, L. Hierarchical Structure and Properties of Graphene Oxide Papers. *J. Appl. Mech.* **2013**, *80*, 040913−1−040913−6.
(25) Bon, S. B.; Valentini, L.; Kenny, J. M. Electric Field Assisted Thermal Annealing Reorganization of Graphene Oxide/Polystyrene Latex Films. *eXPRESS Polym. Lett.* **2011**, *5*, 819−824.
(26) Topsakal, M.; Gürel, H. H.; Ciraci, S. Effects of Charging and Electric Field on Graphene Oxide. *J. Phys. Chem. C* **2013**, *117*, 5943−5952.